Bioorganic & Medicinal Chemistry 20 (2012) 296–304

Contents lists available at SciVerse ScienceDirect

Bioorganic & Medicinal Chemistry

journal homepage: www.elsevier.com/locate/bmc

Quantitative structure–activity relationships of 1,3,4-thiadiazol-2(3*H*)-ones and 1,3,4-oxadiazol-2(3*H*)-ones as human protoporphyrinogen oxidase inhibitors

Yang Zuo [a,†], Sheng-Gang Yang [a,†], Li-Li Jiang [a], Ge-Fei Hao [a], Zhi-Fang Wang [a,b], Qiong-You Wu [a], Zhen Xi [b,*], Guang-Fu Yang [a,*]

[a] Key Laboratory of Pesticide & Chemical Biology of Ministry of Education, College of Chemistry, Central China Normal University, Wuhan 430079, PR China
[b] State Key Laboratory of Elemento-Organic Chemistry, Nankai University, Tianjin 300071, PR China

ARTICLE INFO

Article history:
Received 3 October 2011
Revised 29 October 2011
Accepted 29 October 2011
Available online 10 November 2011

Keywords:
Human protoporphyrinogen oxidase inhibitors
1,3,4-Thiadiazol-2(3*H*)-ones
1,3,4-Oxadiazol-2(3*H*)-ones
QSAR
Molecular docking

ABSTRACT

Protoporphyrinogen oxidase (Protox, EC 1.3.3.4) has attracted great interest during the last decades due to its unique biochemical characteristics and biomedical significance. As a continuation of our research work on the development of new PPO inhibitors, 23 new 1,3,4-thiadiazol-2(3*H*)-ones bearing benzothiazole substructure were designed and synthesized. The in vitro assay indicated that the newly synthesized compounds **1a**–**w** displayed good inhibition activity against human PPO (hPPO) with K_i values ranging from 0.04 μM to 245 μM. To the knowledge, compound **1a**, *O*-ethyl *S*-(5-(5-(*tert*-butyl)-2-oxo-1,3,4-thiadiazol-3(2*H*)-yl)-6-fluorobenzothiazol-2-yl)carbonothioate, with the K_i value of 40 nM, is so far known as the most potent inhibitor against hPPO. Based on the molecular docking and modified molecular mechanics/Poisson–Boltzmann surface area (MM-PBSA) calculations, the quantitative structure–activity relationships of 1,3,4-thiadiazol-2(3*H*)-ones and 1,3,4-oxadiazol-2(3*H*)-one derivatives were established with excellent correlation relationships ($r^2 = 0.81$) between the calculated and experimental binding free energies. Some important insights were also concluded for guiding the future rational design of new hPPO inhibitors with improved potency.

1. Introduction

Protoporphyrinogen-IX oxidase (PPO; EC 1.3.3.4) is the last common enzyme in the biosynthetic pathway leading to heme and chlorophyll synthesis. Its function is to catalyze the transformation from protoporphyrinogen-IX to protoporphyrin-IX.[1–3] In mammals, there is only one isoform of protoporphyrinogen-IX oxidase located on the cytosolic side of the inner mitochondrial membrane.[4–6] However, high plants have two isoforms, plastidic PPO (PPO1) and the mitochondrial PPO (PPO2).[7–11] During the last decades, research interest in PPO has been increasing due to its unique biochemical characteristics and biomedical significance. For example, partial PPO deficiency in humans will cause an inherited disease known as variegated porphyria (VP), whose symptoms include acute abdominal pain, neurological manifestations, and/or cutaneous photosensitivity.[12–16] This disease is relatively common in the white African population of South Africa and be more common in women than in men,[17,18] and may suddenly occur at any age including the adolescent and elderly.[17,19] It is now known that the PPO deficiency is the primary genetic defect in VP,[20] and the activity of PPO in VP patients is reduced by at least 50%.[21] Besides, in the research field of agricultural chemistry, PPO in plants has been identified as one of the most important targets for herbicide discovery since the introduction of herbicidal diphenyl ethers in the 1970s.[22] A great family of structurally diverse PPO inhibitors has been developed as commercial herbicides for weed control in agriculture.[23–30]

In addition, the most potentially useful application of PPO inhibitors is to be used as a treatment for destroying cancer cells via photodynamic therapy (PDT),[31,32] which has been used as a feasible medical technology in the detection and treatment of cancer and other diseases.[33] PDT always involves three key components: a photosensitizer, light, and tissue oxygen.[34] When the PPO is inhibited, the substrate protoporphyrinogen-IX will accumulate and be exported to the cytoplasm where it is slowly oxidized by O_2 in the tumor cells, producing protoporphyrin-IX. In the presence of light, the photosensitive protoporphyrin-IX generates singlet oxygen that causes lipid peroxidation and cell death. Therefore, protoporphyrinogen-IX is an extremely effective photosensitizer after it is activated by PPO inhibitors. Halling et al.[35] showed that PPO inhibitors could activate the photosensitizer protoporphyrinogen-IX and cause its accumulation within tumor cells.

Recently, we reported the high-resolution (1.9 Å) crystal structure of human PPO (hPPO) bound to acifluorfen,[36] which was superimposed onto the PPOs from *Nicotiana tabacum* (mtPPO)[30] and gave an RMSD value of 1.8 Å for 411 Cα atoms.

* Corresponding authors. Tel.: +86 27 67867800; fax: +86 27 67867141 (G.-F.Y.).
E-mail address: gfyang@mail.ccnu.edu.cn (G.-F. Yang).
† Co-first authors.

0968-0896/$ - see front matter © 2011 Elsevier Ltd. All rights reserved.
doi:10.1016/j.bmc.2011.10.079

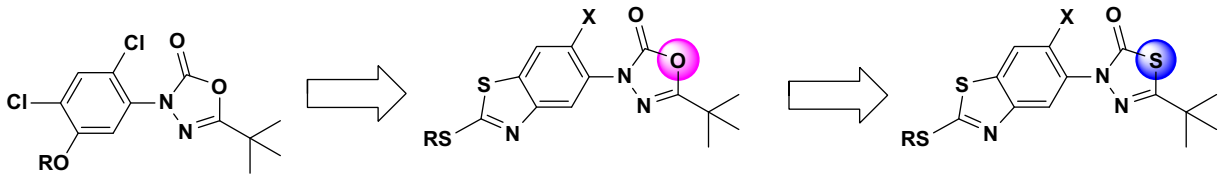

Oxadiazon [R = $CH(CH_3)_2$]
Oxadiargyl [R = CH_2CCH]

1,3,4-Oxadiazol-2(3H)-ones

1a~w
1,3,4-Thiadiazol-2(*3H*)-ones

Scheme 1. Molecular design of the title compound **1a**–**w**.

Although the conformation is highly similar to the FAD-binding and substrate-binding domains, acifluorfen showed much weaker inhibition against hPPO (K_i = 1.71 μM) than against mtPPO (K_i = 0.070 μM). In addition, the K_i values against hPPO of the existing inhibitors are always on the order of micromolar potency, there is so far no nanomolar hPPO inhibitor. Therefore, discovery of new hPPO inhibitor with nanomolar potency is of great interest not only for the elucidating of structural and functional implications of VP-inducing mutations, but for the drug discovery associated with PDT. Previously, we designed and synthesized a series of 1,3,4-oxadiazol-2-(3*H*)-one derivatives as hPPO inhibitors.[37] Very interestingly, some compounds with K_i values against hPPO under 1 μM were successfully discovered. In order to discover new hPPO inhibitors with higher potency, we further designed a series of new 1,3,4-thiadiazol-2(3*H*)-ones by the strategy of oxygen–sulfur bioisosterism substitution (Scheme 1). Very interestingly, a compound with K_i value of 40.00 nM was successfully discovered, to the knowledge, which is so far known as the most potent hPPO inhibitor.

2. Materials and methods

All chemical reagents were commercially available and treated with standard methods before use. Solvents were dried in a routine way and redistilled. ^{1}H NMR spectra was recorded on a Mercury-Plus 400 spectrometer in $CDCl_3$ or DMSO-d_6 with TMS as the internal reference. Mass spectral data were obtained on a MocroMass platform by electrospray ionization (ESI-MS). Elementary analyses were performed on a Vario EL III elementary analysis instrument. Melting points were taken on a Buchi B-545 melting point apparatus and uncorrected. The starting materials of *N′*-(2,4-disubstitutedphenyl)pivalohydrazides (**2a**–**c**) were prepared according to the existing method.[37]

2.1. Preparation of 5-(*tert*-butyl)-3-(2,4-disubstitutedphenyl)-1,3,4-thiadiazol-2(3*H*)-ones (4a–c)

To a refluxing solution of compound **2** in dimethylether (30 mL) was added P_4S_{10} (7.5 mmol). The solvent was evaporated after the reaction accomplished according to the TLC detection. The residue was dissolved in CH_2Cl_2, and washed successively with water (200 mL) and saturated solution of NaCl (200 mL), and then dried over anhydrous magnesium sulfate. After evaporating the solvent, the oil products of **3** was obtained and used directly for the subsequent reaction. The oil intermediate of **3** was dissolved in the solution of CH_2Cl_2, $(C_2H_5)_3N$ (45 mmol) was added. The mixture was cooled to 0 °C, and then a solution of bis(trichloromethyl) carbonate (8.82 g, 30 mmol) in CH_2Cl_2 (50 mL) was added dropwise under a nitrogen atmosphere. The resulted mixture was stirred overnight at room temperature, and then was refluxed for two hours. After cooling, the solution was washed with water (200 mL) and brine (200 mL), then dried, filtered, and concentrated to give the desired oil products of **4a**–**c**.

2.1.1. Data for 4a

Overall yield: 25%; oil; ^{1}H NMR (400 MHz, $CDCl_3$): δ 1.36 (s, 9H, $-C(CH_3)_3$), 7.35–7.44 (m, 2H, Ar-H), 7.54–7.55 (m, 1H, Ar-H); ESI-MS: 302.3 $(M)^+$.

2.1.2. Data for 4b

Overall yield: 36%; oil; ^{1}H NMR (400 MHz, $CDCl_3$): δ 1.35 (s, 9H, $-C(CH_3)_3$), 7.22–7.28 (m, 2H, Ar-H), 7.42–7.46 (m, 1H, Ar-H); ESI-MS: 286.03 $(M)^+$.

2.1.3. Data for 4c

Overall yield: 39%; oil; ^{1}H NMR (400 MHz, $CDCl_3$): δ 1.36 (s, 9H, $-C(CH_3)_3$), 7.12–7.17 (m, 1H, Ar-H), 7.44–7.48 (m, 2H, Ar-H); ESI-MS: 352.6 $(M+Na)^+$.

2.2. Preparation of 5-*tert*-butyl-3-(2,4-disubstituted-5-nitrophenyl)-1,3,4-thiadiazol-2(3*H*)-ones (5a–c)

A solution of HNO_3 (1.07 g, 11.3 mmol) in concentrated H_2SO_4 (2.26 g, 22.6 mmol) was added dropwise to a stirred mixture of **4a**–**c** (11.3 mmol) and concentrated H_2SO_4 (226 mL) in an ice bath. The complete addition took about 15 min. After stirring for 3 h, the solution was slowly poured into a mixture of ice and water (500 mL). The resulted solid was collected by filtration and washed with water (2000 mL), then dried to give to the desired solid products.

2.2.1. Data for 5a

Yield: 65%; oil; ^{1}H NMR (400 MHz, $CDCl_3$): δ 1.37 (s, 9H, $-C(CH_3)_3$), 7.77 (s, 1H, Ar-H), 8.13 (s, 1H, Ar-H). ESI-MS: 369.1 $(M+Na)^+$.

2.2.2. Data for 5b

Yield: 64%; mp: 89–90 °C; ^{1}H NMR (600 MHz, $CDCl_3$): δ 1.37 (s, 9H, $-C(CH_3)_3$), 7.46 (d, *J* = 9.0 Hz, 1H, Ar-H), 8.21 (d, *J* = 6.6 Hz, 1H, Ar-H). ESI-MS: 331.4 $(M)^+$.

2.2.3. Data for 5c

Yield: 80%; mp: 96–97 °C; ^{1}H NMR (400 MHz, $CDCl_3$): δ 1.37 (s, 9H, $-C(CH_3)_3$), 7.70 (d, *J* = 9.6 Hz, 1H, Ar-H), 8.24 (d, *J* = 6.8 Hz, 1H, Ar-H). ESI-MS: 399.1 $(M+Na)^+$.

2.3. Preparation of 3-(5-amino-2,4-disubstitutedphenyl)-5-*tert*-butyl-1,3,4-thiadiazol-2(3*H*)-ones (6a–c):[38]

The powder of Fe was added portionwise to a stirred solution of NH_4Cl (0.83 g), **5a**–**c** (10.4 mmol) in a mixture of EtOH/H_2O (v/v: 10:1, 220 mL) at reflux temperature. After TLC detection showing that reaction finished, the reaction mixture was filtered, concentrated to dryness. The residue was dissolved in water (200 mL) and extracted with EtOAc (200 mL), the organic phase was washed with brine (150 mL), dried, filtered, then concentrated to give the desired oil or solid products.

2.3.1. Data for 6a

Yield: 67%; mp: 102–103 °C; ^{1}H NMR (400 MHz, $CDCl_3$): δ 1.35 (s, 9H, $-C(CH_3)_3$), 4.14 (broad, 2H, $-NH_2$), 6.86 (s, 1H, Ar-H), 7.40 (s, 1H, Ar-H). ESI-MS: 317.7 $(M+H)^+$.

2.3.2. Data for 6b

Yield: 67%; mp: 115–116 °C; ^{1}H NMR (400 MHz, $CDCl_3$): δ 1.35 (s, 9H, $-C(CH_3)_3$), 4.25 (broad, 2H, $-NH_2$), 6.90 (d, J = 6.0 Hz, 1H, Ar-H), 7.18 (d, J = 10.0 Hz, 1H, Ar-H). ESI-MS: 301.6 $(M)^+$.

2.3.3. Data for 6c

Yield: 91%; mp: 96–97 °C; ^{1}H NMR (400 MHz, $CDCl_3$): δ 1.36 (s, 9H, $-C(CH_3)_3$), 3.95 (broad, 2H, $-NH_2$), 6.87 (d, J = 8.0 Hz, 1H, Ar-H), 7.28 (d, J = 10.4 Hz, 1H, Ar-H). ESI-MS: 369.3 $(M+Na)^+$.

2.4. Preparation of 5-*tert*-butyl-3-(6-substituted-2-mercaptobenzo[d]thiazol-5-yl)-1,3,4-thiadiazol-2(3*H*)-ones (7a–c):[39]

A solution of **6a**–**c** (9.45 mmol), potassium *O*-ethyl dithiocarbonate (3.03 g, 18.9 mmol) in 142 mL anhydrous DMF was heated at 120 °C for 3 h. After TLC detection showing that reaction finished, the reaction mixture was evaporated under reduced pressure to remove most solvent and diluted with water (300 ml), and acidified with concentrated HCl solution to induce precipitation (pH 3). Stirring was continued for 10 min. The solid precipitate was collected by filtration, and rinsed with water. The wet filter cake was dried and then purified by flash column chromatography to give the pure products **7a**–**c**.

2.4.1. Data for 7a

Yield: 60%; mp: 170–171 °C; ^{1}H NMR (400 MHz, $CDCl_3$): δ 1.38 (s, 9H, $-C(CH_3)_3$), 7.23 (s, 1H, Ar-H), 7.56 (s, 1H, Ar-H), 10.52 (broad, 1H, –SH). ESI-MS: 357.5 $(M)^+$.

2.4.2. Data for 7b

Yield: 76%; mp: 180–182 °C; ^{1}H NMR (400 MHz, $CDCl_3$): δ 1.40 (s, 9H, $-C(CH_3)_3$), 7.38 (d, J = 8.4 Hz, 1H, Ar-H), 7.45 (d, J = 6.0 Hz, 1H, Ar-H), 10.92 (br, 1H, –SH). ESI-MS: 341.01 $(M)^+$.

2.4.3. Data for 7c

Yield: 68%; mp: 179–180 °C; ^{1}H NMR (400 MHz, $CDCl_3$): δ 1.39 (s, 9H, $-C(CH_3)_3$), 7.21 (s, 1H, Ar-H), 7.72 (s, 1H, Ar-H), 10.45 (broad, 1H, –SH). ESI-MS: 400.2 $(M-H)^-$.

2.5. General synthetic procedure for the target compounds 1a–w

K_2CO_3 powder (0.33 g, 2.4 mmol) was added to a solution of **7a**–**c** (1.2 mmol) in acetone (20 mL). After stirring for 10 min at room temperature, RX (1.8 mmol) in acetone solution was added dropwise to the mixture. The resulted mixture reacted for about 30 min, then filtered, concentrated. The residue was purified via flash chromatography to give the pure products **1a**–**w** in yields of 42–78%.

2.5.1. Data for 1a

Yield: 69%; mp: 146–148 °C. ^{1}H NMR (600 MHz, $CDCl_3$): δ 1.37–1.43 (m, 12H, $-C(CH_3)_3$, $-CH_3$), 4.47 (q, J = 7.2 Hz, 2H, $-OCH_2$), 7.77 (d, J = 8.4 Hz, 1H, Ar-H), 8.15 (d, J = 6.6 Hz, 1H, Ar-H). ESI-MS: 415.4 $(M+2H)^+$. Anal. Calcd for $C_{16}H_{16}FN_3O_3S_3$: 46.47; H, 3.90; N, 10.16. Found: C, 46.73; H, 3.65; N, 10.43.

2.5.2. Data for 1b

Yield: 74%; mp: 111–112 °C. ^{1}H NMR (600 MHz, $CDCl_3$): δ 1.40 (s, 9H, $-C(CH_3)_3$), 3.79 (s, 3H, $-OCH_3$), 4.18 (s, 2H, $-SCH_2$), 7.64 (d, J = 8.4 Hz, 1H, Ar-H), 8.00 (d, J = 6.6 Hz, 1H, Ar-H). ESI-MS: 415.3 $(M+2H)^+$. Anal. Calcd for $C_{16}H_{16}FN_3O_3S_3$: C, 46.47; H, 3.90; N, 10.16. Found: C, 46.74; H, 3.70; N, 10.43.

2.5.3. Data for 1c

Yield: 73%; mp: 124–126 °C. ^{1}H NMR (400 MHz, $CDCl_3$): δ 1.29 (t, J = 7.2 Hz, 3H, $-CH_3$), 1.40 (s, 9H, $-C(CH_3)_3$), 4.17 (s, 2H, $-SCH_2$), 4.23 (q, J = 7.2 Hz, 2H, $-OCH_2$), 7.64 (d, J = 8.4 Hz, 1H, Ar-H), 8.08 (d, J = 6.0 Hz, 1H, Ar-H). ESI-MS: 427.2 $(M)^+$. Anal. Calcd for $C_{17}H_{18}FN_3O_3S_3$: C, 47.76; H, 4.24; N, 9.83. Found: C, 48.02; H, 4.13; N, 9.62.

2.5.4. Data for 1d

Yield: 70%; mp: 86–88 °C. ^{1}H NMR (400 MHz, $CDCl_3$): δ 1.26 (t, J = 7.2 Hz, 3H, $-CH_3$), 1.38 (s, 9H, $-C(CH_3)_3$), 1.71 (d, J = 7.2 Hz, 3H, $-CH(CH_3)$), 4.22 (q, J = 7.2 Hz, 2H, $-OCH_2$), 4.69 (q, J = 7.2 Hz, 1H, –CH), 7.65 (d, J = 8.4 Hz, 1H, Ar-H), 8.00 (d, J = 6.0 Hz, 1H, Ar-H). ESI-MS: 441.4 $(M)^+$. Anal. Calcd for $C_{36}H_{40}BrFN_6O_6S_6$: C, 45.80; H, 4.27; N, 8.90. Found: C, 45.51; H, 4.06; N, 9.20.

2.5.5. Data for 1e

Yield: 78%; mp: 121–123 °C. ^{1}H NMR (400 MHz, $CDCl_3$): δ 1.22 (t, J = 7.2 Hz, 3H, $-CH_3$), 1.40 (s, 9H, $-C(CH_3)_3$), 1.76 (s, 6H, $-SC(CH_3)_2$), 4.20 (t, J = 7.2 Hz, 2H, $-OCH_2$), 7.63 (d, J = 8.4 Hz, 1H, Ar-H), 8.03 (d, J = 6.4 Hz, 1H, Ar-H). ESI-MS: 455.3 $(M)^+$. Anal. Calcd for $C_{19}H_{22}FN_3O_3S_3$: C, 50.09; H, 4.87; N, 9.22. Found: C, 49.86; H, 5.07; N, 9.22.

2.5.6. Data for 1f

Yield: 60%; mp: 86–87 °C. ^{1}H NMR (600 MHz, $CDCl_3$): δ 1.27 (d, J = 6.6 Hz, 6H, $-CH(CH_3)_2$), 1.40 (s, 9H, $-C(CH_3)_3$), 4.13 (s, 2H, $-SCH_2$), 5.08–5.10 (m, 1H, –OCH), 7.64 (d, J = 8.4 Hz, 1H, Ar-H), 7.97 (d, J = 6.6 Hz, 1H, Ar-H). ESI-MS: m/z 441.4 $(M)^+$. Anal. Calcd for $C_{18}H_{20}FN_3O_3S_3$: C, 48.96; H, 4.57; N, 9.52. Found: C, 48.70; H, 4.37; N, 9.35.

2.5.7. Data for 1g

Yield: 49%; mp: 88–89 °C. ^{1}H NMR (600 MHz, $CDCl_3$): δ 0.93 (t, J = 7.2 Hz, 3H, $-CH_3$), 1.40 (s, 9H, $-C(CH_3)_3$), 1.67–1.70 (m, 2H, $-CH_2-$), 4.14 (t, J = 6.6 Hz, 2H, $-OCH_2$), 4.17 (s,2H, $-SCH_2$), 7.64 (d, J = 8.4 Hz, 1H, Ar-H), 7.98 (d, J = 5.4 Hz, 1H, Ar-H). ESI-MS: 442.0 $(M)^+$. Anal. Calcd for $C_{18}H_{20}FN_3O_3S_3$: C, 48.96; H, 4.57; N, 9.52. Found: C, 48.89; H, 4.69; N, 9.36.

2.5.8. Data for 1h

Yield: 63%; mp: 83–84 °C. ^{1}H NMR (600 MHz, $CDCl_3$): δ 1.28 (t, J = 7.2 Hz, 3H, $-CH_3$), 1.40 (s, 9H, $-C(CH_3)_3$), 2.92 (t, J = 7.2 Hz, 2H, $-CH_2CO$), 3.60 (t, J = 7.2 Hz, 2H, $-SCH_2$), 4.19 (q, J = 7.2 Hz, 2H, $-OCH_2$), 7.63 (d, J = 8.4 Hz, 1H, Ar-H), 7.99 (d, J = 6.0 Hz, 1H, Ar-H). ESI-MS: 441.6 $(M)^+$. Anal. Calcd for $C_{18}H_{20}FN_3O_3S_3$: C, 48.96; H, 4.57; N, 9.52. Found: C, 48.73; H, 4.77; N, 9.31.

2.5.9. Data for 1i

Yield: 50%; oil. ^{1}H NMR (400 MHz, $CDCl_3$): δ 1.24 (t, J = 7.2 Hz, 3H, $-CH_3$), 1.40 (s, 9H, $-C(CH_3)_3$), 2.14–2.21 (m, 2H, $-CH_2-$), 2.49 (t, J = 7.2 Hz, 2H, $-CH_2CO$), 3.40 (t, J = 7.2 Hz, 2H, $-SCH_2$), 4.12 (q, J = 7.2 Hz, 2H, $-OCH_2$), 7.63 (d, J = 8.8 Hz, 1H, Ar-H), 7.98 (d, J = 6.4 Hz, 1H, Ar-H). ESI-MS: 455.5 $(M)^+$. Anal. Calcd for $C_{19}H_{22}FN_3O_3S_3$: C, 50.09; H, 4.87; N, 9.22. Found: C, 49.70; H, 4.96; N, 8.93.

2.5.10. Data for 1j

Yield: 60%; mp: 154–157 °C. ^{1}H NMR (600 MHz, $CDCl_3$): δ 1.40 (s, 9H, $-C(CH_3)_3$), 2.31 (s, 1H, –CH), 4.13 (s, 2H, $-SCH_2$), 7.66 (d, J = 9.0 Hz, 1H, Ar-H), 8.05 (d, J = 6.0 Hz, 1H, Ar-H). ESI-MS: 380.2

$(M+H)^+$.Anal. Calcd for $C_{16}H_{14}FN_3OS_3$: C, 50.64; H, 3.72; N, 11.07. Found: C, 50.45; H, 3.50; N, 10.89.

2.5.11. Data for *1k*

Yield: 65%; mp: 137–138 °C. ^{1}H NMR (600 MHz, $CDCl_3$): δ 1.37 (s, 9H, $-C(CH_3)_3$), 1.40 (t, J = 7.2 Hz, 3H, $-CH_3$), 4.45 (q, J = 7.2 Hz, 2H, $-OCH_2$), 8.04 (s, 1H, Ar-H), 8.08 (s, 1H, Ar-H). ESI-MS: 429.9 $(M+H)^+$. Anal. Calcd for $C_{16}H_{16}ClN_3O_3S_3$: C, 44.69; H, 3.75; N, 9.77. Found: C, 44.80; H, 4.00; N, 9.60.

2.5.12. Data for 1l

Yield: 58%; mp: 103–105 °C. ^{1}H NMR (400 MHz, $CDCl_3$): δ 1.25 (t, J = 7.2 Hz, 3H, $-CH_3$), 1.37 (s, 9H, $-C(CH_3)_3$), 4.17 (s, 2H, $-SCH_2$), 4.22 (q, J = 7.2 Hz, 2H, $-OCH_2$), 7.91 (s, 1H, Ar-H), 7.95 (s, 1H, Ar-H). ESI-MS: 443.0 $(M)^+$. Anal. Calcd for $C_{17}H_{18}ClN_3O_3S_3$: C, 45.99; H, 4.09; N, 9.46. Found: C, 46.11; H, 4.42; N, 9.54.

2.5.13. Data for 1m

Yield: 65%; oil. ^{1}H NMR (400 MHz, $CDCl_3$): δ 1.26 (t, J = 7.2 Hz, 3H, $-CH_3$), 1.38 (s, 9H, $-C(CH_3)_3$), 1.71 (d, J = 7.2 Hz, 3H, $-CH(CH_3)$), 4.22 (q, J = 7.2 Hz, 2H, $-OCH_2$), 4.67 (q, J = 7.2 Hz, 1H, –SCH), 7.91 (s, 1H, Ar-H), 7.95 (s, 1H, Ar-H). ESI-MS: 458.0 $(M+H)^+$. Anal. Calcd for $C_{18}H_{20}ClN_3O_3S_3$: C, 47.20; H, 4.40; N, 9.17. Found: C, 47.42; H, 4.69; N, 9.03.

2.5.14. Data for 1n

Yield: 54%; mp: 98–99 °C. ^{1}H NMR (400 MHz, $CDCl_3$): δ 1.21 (t, J = 7.2 Hz, 3H, $-CH_3$), 1.38 (s, 9H, $-C(CH_3)_3$), 1.76 (s, 6H, $-SC(CH_3)_2$), 4.17 (q, J = 7.2 Hz, 2H, $-OCH_2$), 7.92 (s, 1H, Ar-H), 7.98 (s, 1H, Ar-H). ESI-MS: 472.0 $(M+H)^+$. Anal. Calcd for $C_{19}H_{22}ClN_3O_3S_3$: C, 48.34; H, 4.70; N, 8.90. Found: C, 48.50; H, 4.90; N, 8.61.

2.5.15. Data for 1o

Yield: 42%; oil. ^{1}H NMR (400 MHz, $CDCl_3$): δ 1.26 (t, J = 7.2 Hz, 3H, $-CH_3$), 1.38 (s, 9H, $-C(CH_3)_3$), 2.90 (t, J = 7.2 Hz, 2H, $-CH_2CO$), 3.59 (t, J = 7.2 Hz, 2H, $-SCH_2$), 4.16 (q, J = 7.2 Hz, 2H, $-OCH_2$), 7.90 (s, 1H, Ar-H), 7.96 (s, 1H, Ar-H). ESI-MS: 457.4 $(M)^+$. Anal. Calcd for $C_{18}H_{20}ClN_3O_3S_3$: C, 47.20; H, 4.40; N, 9.17. Found: C, 47.43; H, 4.51; N, 9.22.

2.5.16. Data for 1p

Yield: 52%; oil. ^{1}H NMR (400 MHz, $CDCl_3$): δ 1.25 (t, J = 7.2 Hz, 3H, $-CH_3$), 1.37 (s, 9H, $-C(CH_3)_3$), 2.15–2.19 (m, 2H, $-CH_2-$), 2.49 (t, J = 6.8 Hz, 2H, $-CH_2CO$), 3.41 (t, J = 6.8 Hz, 2H, $-SCH_2$), 4.12 (q, J = 7.2 Hz, 2H, $-OCH_2$), 7.90 (s, 1H, Ar-H), 7.95 (s, 1H, Ar-H). ESI-MS: 471.6 $(M+H)^+$. Anal. Calcd for $C_{19}H_{22}ClN_3O_3S_3$: C, 48.34; H, 4.70; N, 8.90. Found: C, 48.63; H, 4.91; N, 8.93.

2.5.17. Data for 1q

Yield: 79%; mp: 111–112 °C. ^{1}H NMR (400 MHz, $CDCl_3$): δ 1.38 (s, 9H, $-C(CH_3)_3$), 2.30 (t, J = 2.4 Hz, 1H, –CH), 4.13 (d, J = 2.4 Hz, 2H, $-SCH_2$), 7.93 (s, 1H, Ar-H), 8.00 (s, 1H, Ar-H). ESI-MS: 395.5 $(M)^+$. Anal. Calcd for $C_{16}H_{14}ClN_3OS_3$: C, 48.53; H, 3.56; N, 10.61. Found: C, 48.60; H, 3.80; N, 10.65.

2.5.18. Data for 1r

Yield: 44%; mp: 104–105 °C. ^{1}H NMR (400 MHz, $CDCl_3$): δ 1.27 (t, J = 7.2 Hz, 3H. $-CH_3$), 1.37 (s, 9H, $-C(CH_3)_3$), 4.16 (s, 2H, $-SCH_2$), 4.22 (q, J = 7.2 Hz, 2H, $-OCH_2$), 7.94 (s, 1H, Ar-H), 8.08 (s, 1H, Ar-H). ESI-MS: 487 $(M-H)^+$, 489.0 $(M+H)^+$. Anal. Calcd for $C_{17}H_{18}BrN_3O_3S_3$: C, 41.80; H, 3.71; N, 8.60. Found: C, 41.62; H, 3.90; N, 8.52.

2.5.19. Data for 1s

Yield: 60%; mp: 88–90 °C. ^{1}H NMR (600 MHz, $CDCl_3$): δ 1.26 (t, J = 7.2 Hz, 3H, $-CH_3$), 1.40 (s, 9H, $-C(CH_3)_3$), 1.71 (d, J = 7.2 Hz, 3H, $-CH(CH_3)$), 4.22 (q, J = 7.2 Hz, 2H, $-OCH_2$), 4.68 (q, J = 7.2 Hz, 1H, –SCH), 7.94 (s, 1H, Ar-H), 8.11 (s, 1H, Ar-H). ESI-MS: 501.9 $(M+H)^+$. Anal. Calcd for $C_{18}H_{20}BrN_3O_3S_3$: C, 43.03; H, 4.01; N, 8.36. Found: C, 43.04; H, 3.85; N, 8.21.

2.5.20. Data for 1t

Yield: 75%; mp: 94–95 °C. ^{1}H NMR (400 MHz, $CDCl_3$): δ 1.21 (t, J = 7.2 Hz, 3H, $-CH_3$), 1.38 (s, 9H, $-C(CH_3)_3$), 1.76 (s, 6H, $-SC(CH_3)_2$), 4.17 (q, J = 7.2 Hz, 2H, $-OCH_2$), 7.98 (s, 1H, Ar-H), 8.10 (s, 1H, Ar-H). ESI-MS: 515.9 $(M+H)^+$. Anal. Calcd for $C_{19}H_{22}BrN_3O_3S_3$: C, 44.18; H, 4.29; N, 8.14. Found: C, 44.11; H, 4.50; N, 8.15.

2.5.21. Data for 1u

Yield: 63%; oil. ^{1}H NMR (400 MHz, $CDCl_3$): δ 1.26 (t, J = 7.2 Hz, 3H, $-CH_3$), 1.38 (s, 9H, $-C(CH_3)_3$), 2.90 (t, J = 6.8 Hz, 2H, $-CH_2CO$), 3.59 (t, J = 6.8 Hz, 2H, $-SCH_2$), 4.16 (q, J = 7.2 Hz, 2H, $-OCH_2$), 7.96 (s, 1H, Ar-H), 8.07 (s, 1H, Ar-H). ESI-MS: 501.8 $(M+H)^+$. Anal. Calcd for $C_{18}H_{20}BrN_3O_3S_3$: C, 43.03; H, 4.01; N, 8.36. Found: C, 42.80; H, 4.30; N, 8.23.

2.5.22. Data for 1v

Yield: 62%; oil. ^{1}H NMR (400 MHz, $CDCl_3$): δ 1.25 (t, J = 7.2 Hz, 3H, $-CH_3$), 1.38 (s, 9H, $-C(CH_3)_3$), 2.13–2.20 (m, 2H, $-CH_2-$), 2.49 (t, J = 7.2 Hz, 2H, $-CH_2CO$), 3.41 (t, J = 7.2 Hz, 2H, $-SCH_2$), 4.12 (q, J = 7.2 Hz, 2H, $-OCH_2$), 7.94 (s, 1H, Ar-H), 8.07 (s, 1H, Ar-H). ESI-MS: 537.8 $(M+Na)^+$. Anal. Calcd for $C_{19}H_{22}BrN_3O_3S_3$: C, 44.18; H, 4.29; N, 8.14. Found: C, 44.44; H, 4.50; N, 8.19.

2.5.23. Data for 1w

Yield: 70%; mp: 131–133 °C. ^{1}H NMR (600 MHz, $CDCl_3$): δ 1.38 (s, 9H, $-C(CH_3)_3$), 2.30 (t, J = 2.4 Hz, 1H, –CH), 4.13 (d, J = 2.4 Hz, 2H, $-SCH_2$), 8.00 (s, 1H, Ar-H), 8.10 (s, 1H, Ar-H). ESI-MS: 440.4 $(M)^+$. Anal. Calcd for $C_{16}H_{14}BrN_3OS_3$: C, 43.64; H, 3.20; N, 9.54. Found: C, 43.83; H, 3.53; N, 9.74.

2.6. X-ray diffraction

A colorless block shaped crystal of **1n** (0.16 × 0.12 × 0.10 mm) was selected and mounted on a Bruker SMART APEX CCD Single Crystal Diffraction System with graphite-monochromated MoK_α radiation (λ = 0.71073 Å) and x-ray provided by a fine-focus sealed tube operated at 50 kV and 30 mA.[40] The crystal determined at 298(2) K was crystallized in the monoclinic, $C2/c$ space group with a = 21.842(2) Å, b = 9.3205(8) Å, c = 24.884(2) Å, β = 115.026(3)°, V = 4590.1(8) Å^3, Z = 4, d_{calcd} = 1.366 g/cm^3 and μ_α(MoK_α) = 0.464 mm^{-1}. Lattice constants were determined with the Bruker *SAINT* software package using peak centers for 6195 reflections.[41] Then a full hemisphere of diffracted intensities with an ω scan width of 0.30° was measured. A total of 14627 integrated reflection intensities having 2.06° < θ < 26.0° were produced using the Bruker program *SAINT* and 4517 of these reflections were unique. The Bruker software package *SHELXTL*[42] was used to solve the structure using 'direct methods' techniques. All stages of weighted full-matrix least-squares refinement were conducted using F_0^2 data with the *SHELXTL* Version 6.10 software package. All the non-hydrogen atoms were found from the difference maps and refined anisotropically. All the hydrogen atoms were located their ideal positions with C–H=0.98 Å (methyl) and 0.93 Å (aromatic) and their isotropic thermal parameters of were fixed at values 1.5 (methyl) or 1.2 (aromatic) times of the equivalent isotropic thermal parameter of their parent carbon atoms. A total of 268 parameters were refined in the refinement. Final agreement factors at convergence are: R_1 = 0.0535, wR_2 = 0.1410 and Gof = 1.068 for 3892 independent reflections with $I > 2\sigma(I)$; R_1 = 0.0606, wR_2 = 0.1463 and Gof = 1.068 for all the 4517 independent reflections. The largest shift/s.u. was 0.000 in the final refinement cycle. The

final difference map had maxima and minima of 0.561 and −0.289 $e^-/Å^3$, respectively.

2.7. Determination of the K_i values of the title compounds against human PPO

The detailed method for enzyme expression, purification and inhibition kinetic analysis has been described previously.[37,43] The kinetic parameters were evaluated by Sigma Plot software 10.0 (SPSS, Chicago, USA). IC_{50} was determined by measuring PPOX activity over a range of inhibitor concentrations at a single substrate concentration. IC_{50} values were calculated by fitting v versus [I] data to a single binding site model described by Eq. 1

$$y = min + \frac{max - min}{1 + 10^{\log IC_{50} - x}} \quad (1)$$

where y is the percentage of maximal rate, max and min are the y values at which the curve levels off, x is the logarithm of inhibitor concentration, and IC_{50} is the inhibitor concentration that elicits 50% of the total inhibition. Calculated K_i value is obtained by applying the following relationship, which exists for competitive inhibition among K_i, K_m, and IC_{50} at any saturating substrate concentration (S).

$$K_i = \frac{IC_{50}}{S/K_m + 1} \quad (2)$$

2.8. Computational simulations and binding free energies calculations

The chemical structures of compounds were constructed by using SYBYL 7.0. The optimized geometries were used as the starting structures for docking study. Docking calculations were performed by using AutoDock4.0.[44] The structures of protein and ligand were prepared with AutoDock Tools.[45] A total of 256 runs were launched for each molecule. Most of the parameters for the docking calculation were set to the default values recommended by the program. For each docked structure, a modified molecular mechanics/Poisson–Boltzmann surface area (MM/PBSA) described before[46] was performed to compare binding energies by analyzing binding strength between the protein and the ligand determined by electrostatic, hydrophilic, and hydrophobic interactions. Before the MM/PBSA calculation, the complex structure was further refined with the steepest descent algorithm first and then the conjugated gradient algorithm by using Amber9 package.[47] The partial atomic charges of ligands were determined using the AM1-BCC method implemented in the Antechamber module of the Amber9 program.[47] During the energy minimization process, the receptor was first fixed and only the ligand was kept free, then the ligand and residue sidechains were kept free. Finally, all atoms of the system were kept free and refined to a convergence of 0.01 kcal/(mol Å). The refined structure was used in the final binding energy calculation. The energy minimization calculations of the fluorine, chlorine and bromine derivatives for the comparison of the dihedral angle between the oxadiazole or thiadiazole and the benzothiazole ring were performed using the GAUSSIAN 03 program.[48]

3. Results and discussion

3.1. Synthetic chemistry of the title compounds

As shown in Scheme 2, the target compounds **1a**–**w** were prepared by a six-step synthetic route. The starting materials of *N*′-(2,4-disubstitutedphenyl)pivalohydrazides (**2a**–**c**) were prepared according to the existing method. Compounds **2a**–**c** were suffered from sulfuration with P_4S_{10} to afford *N*′-(2,4-disubstituted-phenyl)-2,2-dimethylpropanethiohydrazide (**3a**–**c**), which reacted directly without purification with bis(trichloromethyl) carbonate under a nitrogen atmosphere to afford 5-(*tert*-butyl)-3-(2,4-disubstitutedphenyl)-1,3,4-thiadiazol-2(3*H*)-ones (**4a**–**c**). The intermediates of **4a**–**c** reacted with a solution of HNO_3 in concentrated H_2SO_4 to give 5-*tert*-butyl-3-(2,4-disubstituted-5-nitrophenyl)-1,3,4-thiadiazol-2(3*H*)-ones (**5a**–**c**) in yields of 64–80%, which were reduced by Fe powder to afford 3-(5-amino-2,4-disubstitutedphenyl)-5-*tert*-butyl-1,3,4-thiadiazol-2(3*H*)-ones (**6a**–**c**). The intermediates of **6a**–**c** underwent ring-closing reaction with potassium *O*-ethyl carbonodithioate in the DMF solution to produce the key intermediate of 5-*tert*-butyl-3-(6-substituted-2-mercaptobenzo[*d*]thiazol-5-yl)-1,3,4-thiadiazol-2(3*H*)-ones (**7a**–**c**) in acceptable yields (60–76%). Finally, intermediate **7a**–**c** reacted with diverse alkylation reagent to give the target compounds **1a**–**w** in yields of 42–78%. The structures of all intermediates and title compounds were confirmed by elemental analyses, ^{1}H NMR and ESI-MS spectral data. In addition, the crystal structure of **1n** was determined by X-ray diffraction analyses. As can be observed from the structure of **1n** shown in Figure 1, the thiadiazole ring is almost perpendicular to the benzothiazol ring with a dihedral angle of 89.9° between them. In the crystal packing, the adjacent molecules are linked into a one-dimensional chain running parallel to the [010] direction by the C9–H9···O3 (x, 1+y, z, $d_{C9\cdots O3}$ = 3.278(3) Å) hydrogen bond. Further analysis shows that these neighboring chains are joined together into the final three-dimensional network by two $\pi\cdots\pi$ interactions for one between the C7–C12 benzene ring and the S2-involved thiazole ring ($d_{centroid\text{-}to\text{-}centroid}$ = 3.758(2) Å), and the other one between two symmetry-related thiadiazole rings ($d_{centroid\text{-}to\text{-}centroid}$ = 3.950(2) Å).

3.2. Inhibition activity of 1,3,4-thiadiazol-2(3*H*)-ones against hPPO

The k_i values against hPPO of the newly synthesized 1,3,4-thiadiazol-2(3*H*)-ones **1a**–**w** were listed in Table 1. Oxadiazon, a commercial herbicide acting as PPO inhibitor, were used as a control. For the sake of clarity, compounds **1a**–**j**, **1k**–**q** and **1r**–**w** will be named as fluorine, chlorine, and bromine derivatives, respectively through the text. Results as shown in Table 1 indicated that compound **1a** (R = $COOC_2H_5$, K_i = 0.04 μM) displayed the highest hPPO-inhibition activity, about 73-fold higher than oxadiazon (K_i = 2.93 μM). In addition, compound **1k** (R = $COOC_2H_5$, K_i = 0.20 μM) also displayed the highest hPPO inhibition activity within the chlorine derivatives. These results showed that $COOC_2H_5$ might be the best substituent among the investigated R groups. As far as the same R group be concerned, fluorine derivatives (compounds **1a**–**1j**) always displayed much higher hPPO-inhibition activity than chlorine derivatives (compounds **1k**–**1q**) and bromine derivatives (compounds **1r**–**1w**). However, the chlorine derivative **1o** (K_i = 1.28 μM), whose R group is $CH_2CH_2COOCH_2CH_3$, is an exception and became the stronger hPPO inhibitor than the corresponding fluorine derivative **1h** (K_i = 9.26 μM) and bromine derivative **1v** (K_i = 27.5 μM).

In order to understand the structure–activity relationships, we compared the hPPO-inhibition activity of compounds **1a**–**w** with their corresponding 1,3,4-oxadiazol-2(3*H*)-one derivatives which were previously synthesized.[37] As shown in Table 1, apart from compounds **1a**– **c** and **1k**, other compound **1** displayed lower hPPO-inhibition activity than their corresponding 1,3,4-oxadiazol-2(3*H*)-one derivatives. Very interestingly, for the 1,3,4-oxadiazol-2(3*H*)-one derivatives, the fluorine derivative sometimes displayed higher activity than the corresponding chlorine derivatives containing the same R group, while sometimes lower activity than the corresponding chlorine derivatives. However, in most cases,

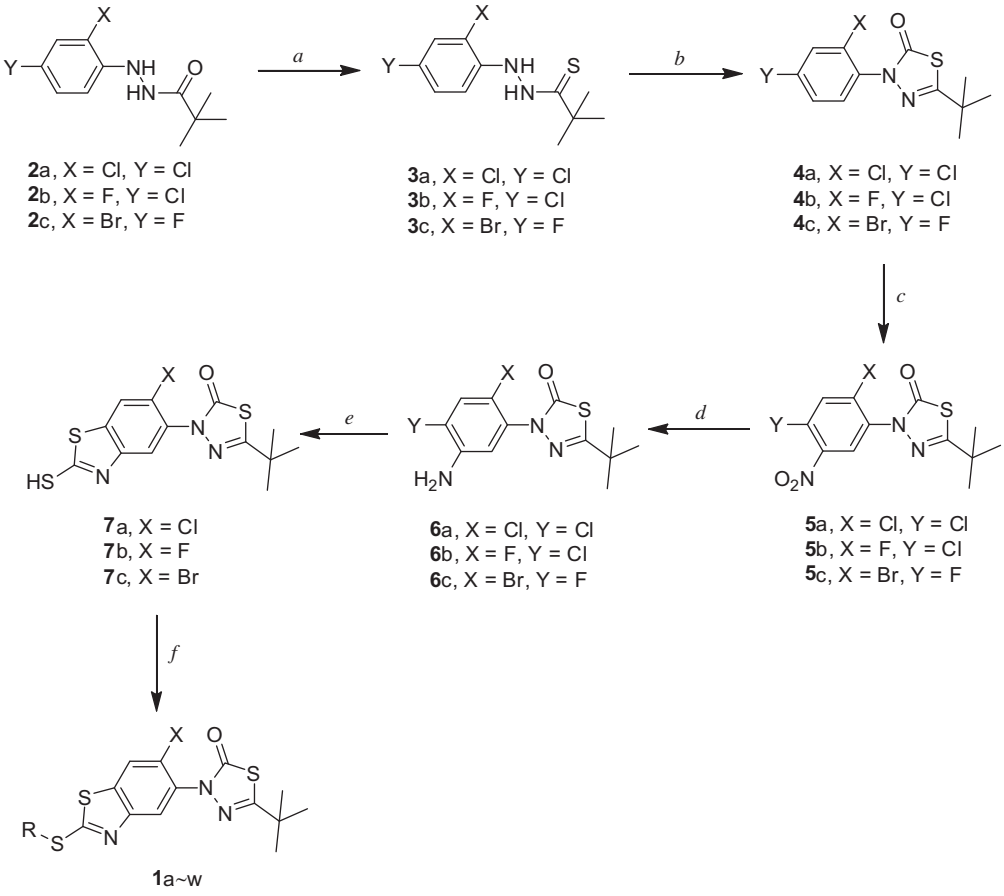

Reagents and conditions: *a*, P_4S_{10}, DME, reflux; *b*, $(COCl_2)_3$, NEt_3, toluene, N_2; *c*, HNO_3/H_2SO_4, 0^0C; *d*, iron powder, NH_4Cl, $EtOH/H_2O$, reflux; *e*, EtOC(S)SK, DMF, relux, con. HCl; *f* , acetone, K_2CO_3, RX, rt.

Scheme 2. Synthetic route for the title compound **1a–w**.

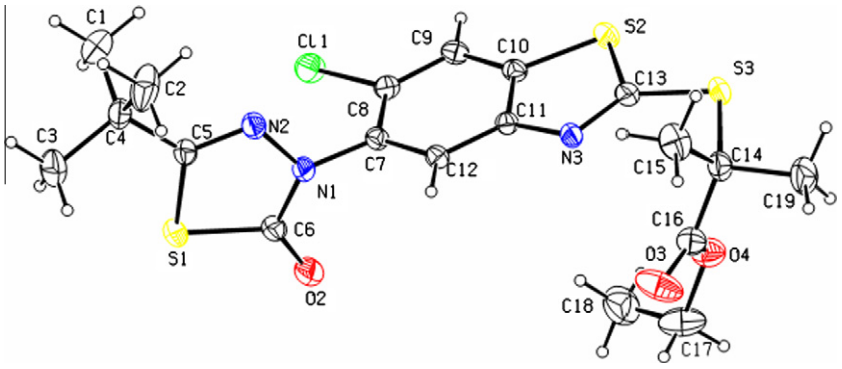

Figure 1. Crystal structure of compound **1n**.

the fluorine derivatives of 1,3,4-thiadiazol-2(3*H*)-ones displayed higher activity than the corresponding chlorine derivatives. One similarity is that the bromine derivatives of 1,3,4-oxadiazol-2(3*H*)-one and 1,3,4-thiadiazol-2(3*H*)-one always displayed the lowest hPPO-inhibition activity.

3.3. Binding free energies calculation and quantitative structure–activity relationships

Summarized in Table 1 are the energetic results obtained from the binding free energy calculations. The binding free energies calculated for all ligands range from −9.28 to −14.01 kcal/mol, while the experimental binding free energies range from −4.93 to −10.10 kcal/mol. Obviously, the MM-PBSA calculations overestimated the absolute binding affinities of the ligands with the enzyme. However, the calculated values are expected to reflect the relative change of the binding affinities of the compounds. Qualitatively in comparison with the experimental data, there is a good linear correlation (r^2 = 0.81) between ΔG_{cal} and ΔG_{exp} derived from the experimental data (Fig. 2), suggesting that the computational models constructed and tested in this study should be reliable.

Because the oxygen atom in oxadiazole is more electronegative but less bulky than sulfur atom in thiadiazole, compared with the oxadiazole ring, the thiadiazole ring might have different

Table 1
The K_i values (μM) of compounds **1** and **8** against hPPO, and their calculated binding free energies (ΔG_{cal}, kcal/mol)

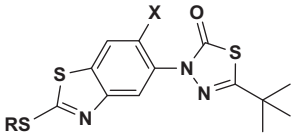

1a~w

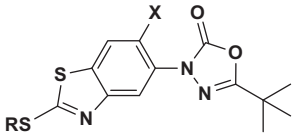

8a~w

No.	X	R	ΔE_{ELE}	ΔE_{VDW}	ΔE_{GAS}	ΔG_{SOL}	ΔG_{PB}	$-T\Delta S$	ΔG_{cal}	K_i[a]	ΔG_{exp}[b]
1a	F	$COOCH_2CH_3$	−17.84	−56.43	−74.27	35.81	−38.45	24.44	−14.01	0.04	−10.10
1b	F	CH_2COOCH_3	−24.12	−54.44	−78.58	36.00	−42.56	30.57	−11.99	3.05	−7.53
1c	F	$CH_2COOCH_2CH_3$	−20.03	−58.75	−78.78	37.61	−41.17	27.60	−13.57	0.34	−8.84
1d	F	$CH(CH)_3COOC_2H_5$	−25.46	−56.51	−81.97	37.72	−44.25	32.76	−11.49	5.89	−7.14
1e	F	$C(CH_3)_2COOC_2H_5$	−24.35	−57.67	−82.02	34.01	−48.01	35.44	−12.57	3.46	−7.46
1f	F	$CH_2COOCH(CH_3)_2$	−24.74	−51.85	−76.58	34.97	−41.61	27.96	−13.65	1.26	−8.06
1g	F	$CH_2COOC_3H_7$	−25.24	−57.47	−82.71	40.34	−42.38	30.11	−12.27	1.31	−8.04
1h	F	$CH_2CH_2COOC_2H_5$	−27.44	−55.68	−83.12	39.09	−44.04	31.92	−12.12	9.26	−6.88
1i	F	$CH_2(CH_2)_2COOC_2H_5$	−25.88	−58.94	−84.82	37.57	−47.25	35.45	−11.80	8.67	−6.91
1j	F	CH_2CCH	−6.40	−52.52	−58.92	20.12	−38.79	27.44	−11.35	9.73	−6.85
1k	Cl	$COOC_2H_5$	−15.16	−58.27	−73.43	33.04	−40.39	26.57	−13.82	0.20	−9.15
1l	Cl	$CH_2COOC_2H_5$	−21.44	−56.39	−77.83	32.88	−44.95	32.75	−12.20	5.82	−7.15
1m	Cl	$CH(CH_3)COOC_2H_5$	−24.90	−58.09	−82.99	36.46	−46.54	34.72	−11.83	12.00	−6.72
1n	Cl	$C(CH_3)_2COOC_2H_5$	−16.02	−60.79	−76.81	32.35	−44.45	33.49	−10.96	34.4	−6.10
1o	Cl	$CH_2CH_2COOC_2H_5$	−22.85	−62.40	−85.25	40.02	−45.23	32.63	−12.60	1.28	−8.05
1p	Cl	$CH_2(CH_2)_2COOC_2H_5$	−28.48	−61.14	−89.62	44.71	−44.90	34.25	−10.65	17.70	−6.49
1q	Cl	CH_2CCH	−7.10	−54.24	−61.34	21.46	−39.88	28.14	−11.74	21.40	−6.38
1r	Br	$CH_2COOC_2H_5$	−23.29	−55.90	−79.19	35.44	−43.75	32.83	−10.92	15.60	−6.57
1s	Br	$CH(CH_3)COOC_2H_5$	−19.51	−56.45	−75.96	32.61	−43.36	34.08	−9.28	173.0	−5.14
1t	Br	$C(CH_3)_2COOC_2H_5$	−21.73	−57.82	−79.55	35.24	−44.31	32.79	−11.52	43.50	−5.96
1u	Br	$CH_2CH_2COOC_2H_5$	−22.64	−61.90	−84.54	40.46	−44.08	33.26	−10.82	27.50	−6.23
1v	Br	$CH_2(CH_2)_2COOC_2H_5$	−20.42	−53.69	−74.11	35.53	−38.58	28.60	−9.98	2450	−4.93
1w	Br	CH_2CCH	−11.16	−57.85	−69.01	29.19	−39.82	28.00	−11.82	20.70	−6.40
8a	F	$COOCH_2CH_3$	−15.57	−53.67	−69.24	31.57	−37.68	24.09	−13.59	0.72	−8.39
8b	F	CH_2COOCH_3	−23.99	−54.17	−78.16	35.66	−42.50	30.47	−12.03	3.99	−7.38
8c	F	$CH_2COOCH_2CH_3$	−24.27	−55.53	−79.79	35.85	−43.95	30.95	−13.00	1.58	−7.92
8d	F	$CH(CH)_3COOC_2H_5$	−25.07	−56.22	−81.28	36.89	−44.39	31.59	−12.80	1.42	−7.99
8e	F	$C(CH_3)_2COOC_2H_5$	−22.29	−57.25	−79.55	30.81	−48.73	36.09	−12.64	1.54	−7.94
8f	F	$CH_2COOCH(CH_3)_2$	−23.58	−52.65	−76.23	35.11	−41.12	27.71	−13.41	1.17	−8.10
8g	F	$CH_2COOC_3H_7$	−23.93	−58.22	−82.15	37.23	−44.91	31.92	−12.99	0.70	−8.41
8h	F	$CH_2CH_2COOC_2H_5$	−24.67	−57.37	−82.04	36.20	−45.84	31.74	−14.10	0.32	−8.87
8i	F	$CH_2(CH_2)_2COOC_2H_5$	−26.4	−57.14	−83.54	37.85	−45.69	31.87	−13.82	0.36	−8.80
8j	F	CH_2CCH	−4.03	−54.92	−58.95	16.24	−42.71	30.10	−12.61	1.92	−7.81
8k	Cl	$COOC_2H_5$	−15.97	−57.29	−73.26	31.95	−41.31	27.56	−13.78	0.33	−8.85
8l	Cl	$CH_2COOC_2H_5$	−24.62	−56.41	−81.03	37.98	−43.05	29.46	−13.59	1.07	−8.16
8m	Cl	$CH(CH_3)COOC_2H_5$	−21.7	−56.39	−78.09	32.15	−45.95	32.39	−13.57	1.69	−7.88
8n	Cl	$C(CH_3)_2COOC_2H_5$	−25.6	−58.33	−83.93	37.21	−46.73	33.71	−13.02	1.35	−8.02
8o	Cl	$CH_2CH_2COOC_2H_5$	−27.94	−57.63	−85.57	37.55	−48.02	34.20	−13.82	0.25	−9.02
8p	Cl	$CH_2(CH_2)_2COOC_2H_5$	−28.76	−60.50	−89.27	44.76	−44.50	31.95	−12.56	2.02	−7.78
8q	Cl	CH_2CCH	−6.41	−52.92	−59.33	19.22	−40.11	28.48	−11.63	8.61	−6.92
8r	Br	$CH_2COOC_2H_5$	−24.11	−53.23	−77.34	31.65	−45.69	33.12	−12.57	6.96	−7.05
8s	Br	$CH(CH_3)COOC_2H_5$	−20.86	−55.15	−76.01	31.62	−44.39	32.30	−12.09	8.13	−6.95
8t	Br	$C(CH_3)_2COOC_2H_5$	−21.21	−57.86	−79.07	31.16	−47.91	35.24	−12.67	1.58	−7.92
8u	Br	$CH_2CH_2COOC_2H_5$	−24.82	−56.71	−81.54	36.15	−45.39	32.36	−13.03	1.69	−7.88
8v	Br	$CH_2(CH_2)_2COOC_2H_5$	−26.4	−57.92	−84.31	38.72	−45.60	35.57	−10.03	5.83	−7.15
8w	Br	CH_2CCH	−6.58	−52.16	−58.73	20.17	−38.56	27.51	−11.05	11.12	−6.77
Oxadiazon										2.93	

[a] The K_i values of compounds **8a–w** against hPPO was taken from Ref. 37.
[b] $\Delta G_{exp} = -RT\ln K_i$.

interaction with the surrounding residues, which can be reflected by the energy decomposition of **1a–w** and **8a–w**. As shown in Table 1, compound **1a** is the most potent inhibitor, displaying about 18-times higher PPO-inhibition activity than the corresponding 1,3,4-oxadiazol-2(3*H*)-one **8a**. In order to understand the molecular basis why compound **1a** displayed higher activity than **8a**, we compared their binding modes. As shown in Figure 3, we found that the simulated binding modes of compounds **1a** and **8a** were very similar. The oxadiazole and thiadiazole rings were sandwiched between the residues of M368 and G169, and formed hydrophobic interaction with these two residues. The benzothiazole moiety of compounds **1a** and **8a** was located between the residues of V347 and L334, and formed a T–π interaction with the side chain of F331. In addition, the side chain of the benzothiazole cycle formed hydrogen bond interactions with R97. As listed in Table 1, the binding free energies (ΔG_{cal}) of compounds **1a** and **8a** are, respectively, −14.01 and −13.59 kcal/mol, which are qualitatively in good agreement with the experimentally-derived binding free energies (ΔG_{exp}) (−10.10 and −8.39 kcal/mol). The energy component analysis showed that the difference came from the electrostatic and van der Waals interactions, and solvation effect. Compound **1a** had a stronger electrostatic (−17.84 kcal/mol) and van der Waals interactions (−56.43 kcal/mol) than compound **8a** (−15.57 and −53.67 kcal/mol) of, but higher solvation (35.81 kcal/mol) penalty than that (31.57 kcal/mol) of compound **8a**. From Figure 3, we can also conclude that replacement of oxadiazole by thiadiazole

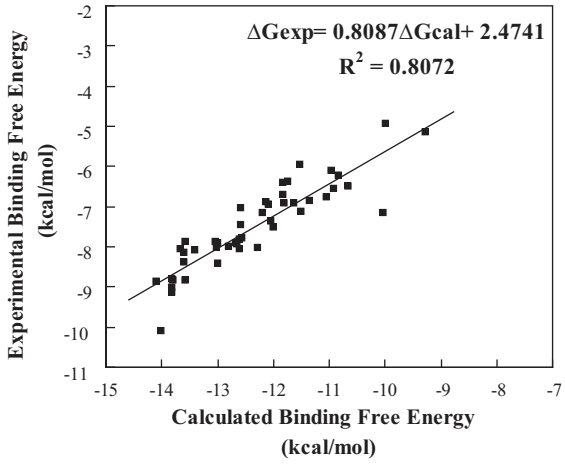

Figure 2. Correlation between the calculated and experimental binding free energies.

resulted in a stronger hydrogen bond interaction between R97 and the oxygen atom of the side-chain ester group.

Very interestingly, when the carbonyl oxygen atom rather than the ester oxygen atom formed hydrogen bonds with R97, the binding affinity will not be improved. For example, compounds **1h** and **8h** displayed lower hPPO-inhibition activity than compounds **1a** and **8a**, respectively. As shown in Table 1, after inserting two more carbon atoms between the carbonyl and sulfur atom, the hydrogen bond interactions between the carbonyl oxygen atom and R97 were improved significantly, and their electrostatic interaction energies were also improved. However, due to their longer side chain, the entropy penalties of **1h** and **8h** are 31.92 kcal/mol and 31.74 kcal/mol, which are greatly higher than that of compounds **1a** (24.44 kcal/mol) and **8a** (24.09 kcal/mol), respectively.

In addition, as shown in Figure 4, we also compared the dihedral angle between the oxadiazole or thiadiazole ring and the benzothiazole ring of the energy-minimized structures of the fluorine, chlorine and bromine derivatives based on HF/6–31G* level. The results indicated that the dihedral angle of fluorine derivatives is very similar to that of 4-bromo-3-(5′-carboxy-4′-chloro-2′-fluorophenyl)-1-methyl-5-trifluoro-methyl-pyrazol (INH) in the crystal structure of tobacco (*N. tabacum*) PPO. However, the dihedral angles of chlorine and bromine derivatives are significantly different from that of INH. That means that there is a little energy difference between the energy-minimized structures and the bioactive conformation of fluorine derivatives. However, the chlorine and bromine derivatives need to overcome a larger energy barrier when they bind to the enzyme.

4. Conclusion

In summary, a series of 1,3,4-thiadiazol-2(3*H*)-ones containing benzothiazole substructure were designed and synthesized as potential hPPO inhibitors. The in vitro results indicated that compound **1a**, *O*-ethyl *S*-(5-(5-(*tert*-butyl)-2-oxo-1,3,4-thiadiazol-3(2*H*)-yl)-6-fluorobenzo-thiazol-2-yl)carbonothioate, displayed the highest PPO-inhibition activity (k_i = 40 nM), about 73-fold higher than oxadiazon. To our knowledge, it is so far the most potent hPPO inhibitor. The results of computational simulations indicated that compound **1a** has a very similar binding mode as its corresponding 1,3,4-oxadiazol-2(3*H*)-one derivative **8a**. The binding free energy calculations showed that the higher activity of compound **1a** is mainly from the stronger electrostatic and van der Waals interactions. According to the established computational models, we can conclude that: (1) Improving the hydrogen bond interaction between R97 and the side chain of inhibitors should be favorable to the binding affinity. (2) Too long side chain will led to higher conformation flexibility of inhibitors and decrease the binding affinity. (3) The dihedral angle between the oxadiazole or thiadiazole and the benzothiazole ring is an important factor which should be taken into account when designing new inhibitors. We believe that these insights will be helpful for the future rational design of novel hPPO inhibitors with improved potency.

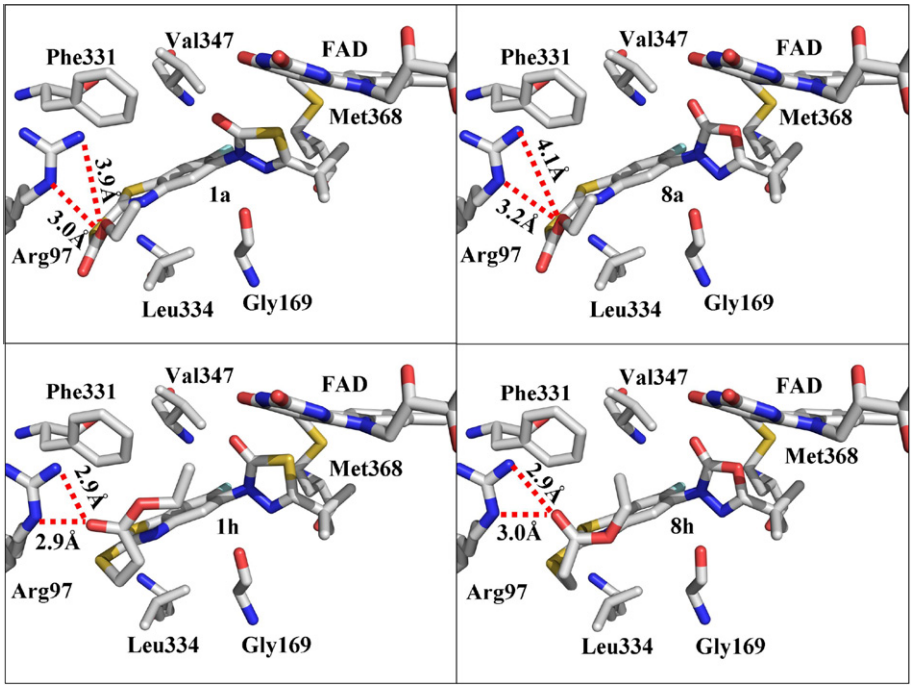

Figure 3. Computational simulated binding models of compounds **1a**, **1h**, **8a**, and **8h**.

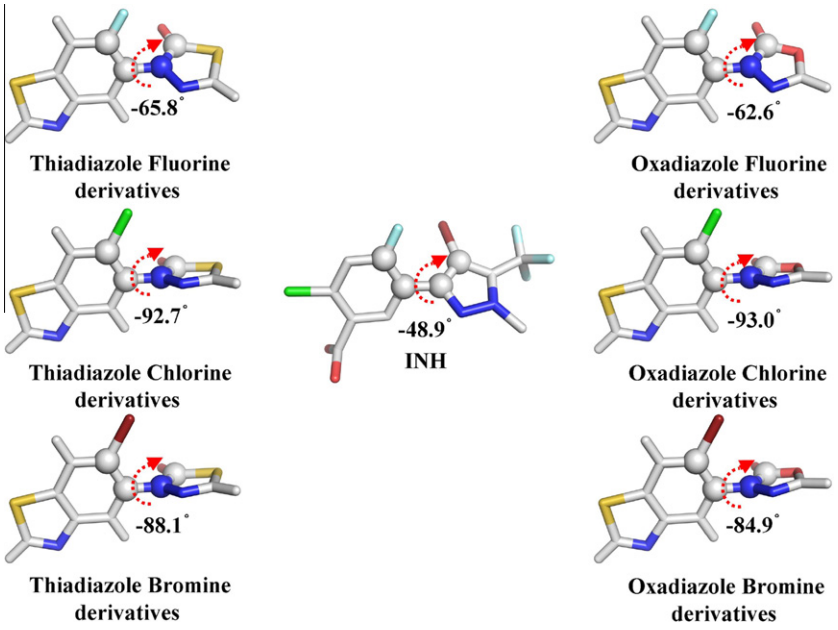

Figure 4. Comparison of the dihedral angles between the oxadiazole or thiadiazole rings and the benzothiazole ring of the fluorine, chlorine and bromine derivatives. The energy minimization was performed at HF/6–31G* level. The conformation of INH was taken from its PPO complex crystal structure.

Acknowledgments

We should thank the financial support from the National Basic Research Program of China (2010CB126103), and the National Natural Science Foundation of China (Nos. 20925206, 21002038 and 20932005), and the PCSIRT (No. IRT0953).

References and notes

1. Gerald, S. M. *Bot. Rev.* **1966**, *32*, 56.
2. Poulson, R.; Polglase, W. J. *J. Biol. Chem.* **1975**, *250*, 1269.
3. Poulson, R. *J. Biol. Chem.* **1976**, *251*, 3730.
4. Deybach, J. C.; Da Silva, V.; Grandchamp, B.; Nordmann, Y. *Eur. J. Biochem.* **1985**, *149*, 431.
5. Ferreira, G. C.; Andrew, T. L.; Karr, S. W.; Dailey, H. A. *J. Biol. Chem.* **1988**, *263*, 3835.
6. Ferreira, G. C.; Dailey, H. A. *Biochem. J.* **1988**, *250*, 597.
7. Beale, S. I. *Photosynth. Res.* **1999**, *60*, 43.
8. Heinemann, I. U.; Diekmann, N.; Masoumi, A.; Koch, M.; Messerschmidt, A.; Jahn, M.; Jahn, D. *Biochem. J.* **2007**, *402*, 575.
9. Jacobs, J. M.; Jacobs, N. J. *Arch. Biochem. Biophys.* **1984**, *229*, 312.
10. Jung, S.; Lee, Y.; Yang, K.; Lee, S. B.; Jang, S. M.; Ha, S. B.; Back, K. *Plant Cell Environ.* **2004**, *27*, 1436.
11. Lermontova, I.; Kruse, E.; Mock, H. P.; Grimm, B. *Proc. Natl. Acad. Sci. U.S.A.* **1997**, *94*, 8895.
12. Brenner, D. A.; Bloomer, J. R. *N. Engl. J. Med.* **1980**, *302*, 765.
13. Deybach, J. C.; De Verneuil, H.; Nordmann, Y. *Hum. Genet.* **1981**, *58*, 425.
14. Meissner, P. N.; Day, R. S.; Moore, M. R.; Disler, P. B.; Harley, E. *Eur. J. Clin. Invest.* **1986**, *16*, 257.
15. Nordmann, Y.; Puy, H. *Clin. Chim. Acta.* **2002**, *325*, 17.
16. Whatley, S. D.; Puy, H.; Morgan, R. R.; Robreau, A. M.; Roberts, A. G.; Nordmann, Y.; Elder, G. H.; Deybach, J. C. *Am. J. Hum. Genet.* **1999**, *65*, 984.
17. Dean, G. *The porphyrias: A story of inheritance and environment*, 2nd ed.; Pitman Medical: London, 1971.
18. Jenkins, T. *Nat. Genet.* **1996**, *13*, 7.
19. Day, R. S. *Semin. Dermatol.* **1986**, *5*, 138.
20. Deybach, J. C.; Puy, H.; Robreau, A. M.; Lamoril, J.; Da Silva, V.; Grandchamp, B.; Nordmann, Y. *Hum. Mol. Genet.* **1996**, *5*, 407.
21. Meissner, P. N.; Dailey, T. A.; Hift, R. J.; Ziman, M.; Corrigall, A. V.; Roberts, A. G.; Meissner, D. M.; Kirsch, R. E.; Dailey, H. A. *Nat. Genet.* **1996**, *13*, 95.
22. Duke, S. O.; Lydon, J.; Becerril, J. M.; Sherman, T. D.; Lehnen, L. P., Jr.; Matsumoto, H. *Weed Sci.* **1991**, 465.
23. Liu, Y. X.; Cui, Z. P.; Liu, B.; Cai, B. L.; Li, Y. H.; Wang, Q. M. *J. Agric. Food Chem.* **2009**, *58*, 2685.
24. Nagano, E.; Hashimoto, S.; Yoshida, R.; Matsumoto, H.; Oshio, H.; Kamoshita, K. EP Patent 61,741, 1982.
25. Gitsopoulos, T. K.; Froud-Williams, R. J. *Weed Res.* **2004**, *44*, 329.
26. Hiraki, M.; Ohki, S.; Sato, Y.; Jablonkai, I.; Boger, P.; Wakabayashi, K. *Pestic. Biochem. Phys.* **2001**, *70*, 159.
27. Theodoridis, G. U.S. Patent 5798,316, 1989.
28. Theodoridis, G.; Princetons, N. J. U.S. Patent 4818,275, 1989.
29. Corradi, H. R.; Corrigall, A. V.; Boix, E.; Mohan, C. G.; Sturrock, E. D.; Meissner, P. N.; Acharya, K. R. *J. Biol. Chem.* **2006**, *281*, 38625.
30. Koch, M.; Breithaupt, C.; Kiefersauer, R.; Freigang, J.; Huber, R.; Messerschmidt, A. *J. EMBO* **2004**, *23*, 1720.
31. Duke, S. O.; Rebeiz, C. A. In *ACS Symposium Series*; American Chemical Society: Washington, DC, 1994; Vol. 559, p 71.
32. Fingar, V. H.; Wieman, T. J.; McMahon, K. S.; Haydon, P. S.; Halling, B. P.; Yuhas, D. A.; Winkelman, J. W. *Cancer Res.* **1997**, *57*, 4551.
33. Volker, A.; Burkhard, G. U.S. Patent 20050049228, 2005.
34. Dolmans, D. E. J. G. J.; Fukumura, D.; Jain, R. K. *Nat. Rev. Cancer* **2003**, *3*, 380.
35. Halling, B. P.; Yuhas, D. A.; Fingar, V. F.; Winkelmann, J. W. *Protophyrinogen Oxidase Inhibitors for Tumor Therapy, in Porphyric Pesticides: Chemistry, Toxicology and Pharmaceutical Applications*; American Chemical Society: Washington, DC, 1994.
36. Qin, X. H.; Tan, Y.; Wang, L. L.; Wang, Z. F.; Wang, B. F.; Wen, X.; Yang, G. F.; Xi, Z.; Shen, Y. Q. *FASEB J.* **2011**, *25*, 653.
37. Jiang, L. L.; Tan, Y.; Zhu, X. L.; Wang, Z. F.; Zuo, Y.; Chen, Q.; Xi, Z.; Yang, G. F. *J. Agric. Food Chem.* **2010**, *58*, 2643.
38. Bosch, J.; Roca, T.; Catena, J. L.; Farrerons, C.; Miquel, I. *Synthesis* **2000**, 721.
39. Zhu, L.; Zhang, M. B.; Dai, M. *J. Heterocycl. Chem.* **2005**, *42*, 727.
40. Bruker. SMART (Version 5.628), Bruker AXS, Inc., Madison, Wisconsin, USA, 2001.
41. Bruker. SAINT-Plus (Version 6.45), Bruker AXS, Inc., Madison, Wisconsin, USA, 2001.
42. Sheldrick, G. M. *Acta Crystallogr., Sect. A* **2008**, *64*, 112.
43. Tan, Y.; Sun, L.; Xi, Z.; Yang, G. F.; Jiang, D. Q.; Yan, X. P.; Yang, X.; Li, H. Y. *Anal. Biochem.* **2008**, *383*, 200.
44. Morris, G. M.; Goodsell, D. S.; Halliday, R. S.; Huey, R.; Hart, W. E.; Belew, R. K.; Olson, A. J. *J. Comput. Chem.* **1998**, *19*, 1639.
45. Sanner, M. F. *J. Mol. Graphics Modell.* **1999**, *17*, 57.
46. Xiong, Y.; Li, Y.; He, H.; Zhan, C. G. *Bioorg. Med. Chem. Lett.* **2007**, *17*, 5186.
47. Case, D. A.; Darden, T. A.; Cheatham; Iii, T. E.; Simmerling, C. L.; Wang, J.; Duke, R. E.; Luo, R.; Merz, K. M.; Pearlman, D. A.; Crowley, M. AMBER 9, University of California, San Francisco, 2006.
48. Frisch, M. J.; Trucks, G. W.; Schlegel, H. B.; Scuseria, G. E.; Robb, M. A.; Cheeseman, J. R.; Montgomery, J. A.; Vreven, T.; Kudin, K. N.; Burant, J. C.; Millam, J. M.; Iyengar, S. S.; Tomasi, J.; Barone, V.; Mennucci, B.; Cossi, M.; Scalmani, G.; Rega, N.; Petersson, G. A.; Nakatsuji, H.; Hada, M.; Ehara, M.; Toyota, K.; Fukuda, R.; Hasegawa, J.; Ishida, M.; Nakajima, T.; Honda, Y.; Kitao, O.; Nakai, H.; Klene, M.; Li, X.; Knox, J. E.; Hratchian, H. P.; Cross, J. B.; Bakken, V.; Adamo, C.; Jaramillo, J.; Gomperts, R.; Stratmann, R. E.; Yazyev, O.; Austin, A. J.; Cammi, R.; Pomelli, C.; Ochterski, J. W.; Ayala, P. Y.; Morokuma, K.; Voth, G. A.; Salvador, P.; Dannenberg, J. J.; Zakrzewski, V. G.; Dapprich, S.; Daniels, A. D.; Strain, M. C.; Farkas, O.; Malick, D. K.; Rabuck, A. D.; Raghava-chari, K.; Foresman, J. B.; Ortiz, J. V.; Cui, Q.; Baboul, A. G.; Clifford, S.; Cioslowski, J.; Stefanov, B. B.; Liu, G.; Liashenko, A.; Piskorz, P.; Komaromi, I.; Martin, R. L.; Fox, D. J.; Keith, T.; Al-Laham, M. A.; Peng, C. Y.; Nanayakkara, A.; Challacombe, M.; Gill, P. M. W.; Johnson, B.; Chen, W.; Wong, M. W.; Gonzalez, C.; Pople, J. A. Gaussian 03, revision B-03, Gaussian, Inc.: Pittsburgh, PA, 2003.